

Comparative study of boron and neon injections on divertor heat fluxes using SOLPS-ITER simulations

Lei Peng(彭磊), Zhen Sun(孙震), Ji-Zhong Sun(孙继忠), Rajesh Maingi, Fang Gao(高放), Hua-Yi Chang(常华溢), Wei-Kang Wang(汪炜康), and Jin-Yuan Liu(刘金远)

Citation: Chin. Phys. B, 2024, 33 (**11**): 115201. DOI: 10.1088/1674-1056/ad711e
Journal homepage: http://cpb.iphy.ac.cn; http://iopscience.iop.org/cpb

What follows is a list of articles you may be interested in

Calculation and prediction of divertor detachment via impurity seeding by using one-dimensional model

Wen-Jie Zhou(周文杰), Xiao-Ju Liu(刘晓菊), Xiao-He Wu(邬潇河), Bang Li(李邦), Qi-Qi Shi(石奇奇), Hao-Chen Fan(樊皓尘), Yan-Jie Yang(杨艳杰), and Guo-Qiang Li(李国强)
Chin. Phys. B, 2024, 33 (**8**): 085205. DOI: 10.1088/1674-1056/ad426a

Simulation of deuterium pellet ablation and deposition in the EAST tokamak with HPI2 code

Da-Zheng Li(李大正), Jie Zhang(张洁), Ji-Lei Hou(侯吉磊), Mao Li(李懋), and Ji-Zhong Sun(孙继忠)
Chin. Phys. B, 2024, 33 (**4**): 045204. DOI: 10.1088/1674-1056/ad1e68

Evolution of the high-field-side radiation belts during the neon seeding plasma discharge in EAST tokamak

Ji-Chan Xu(许吉禅), Liang Wang(王亮), Guo-Sheng Xu(徐国盛), Yan-Min Duan(段艳敏), Ling-Yi Meng(孟令义), Ke-Dong Li(李克栋), Fang Ding(丁芳), Rui-Rong Liang(梁瑞荣), Jian-Bin Liu(刘建斌), and EAST Team
Chin. Phys. B, 2022, 31 (**10**): 105203. DOI: 10.1088/1674-1056/ac935a

Gaussian process tomography based on Bayesian data analysis for soft x-ray and AXUV diagnostics on EAST

Yan Chao(晁燕), Liqing Xu(徐立清), Liqun Hu(胡立群), Yanmin Duan(段艳敏), Tianbo Wang(王天博), Yi Yuan(原毅), Yongkuan Zhang(张永宽)
Chin. Phys. B, 2020, 29 (**9**): 095201. DOI: 10.1088/1674-1056/aba2e4

Observation of deuterium molecule emission spectra under an active feedback control of H-mod plasma divertor detachment experiment on the EAST tokamak

Wei Gao(高伟), Juan Huang(黄娟), Jichan Xu(许吉禅), Liang Wang(王亮), Jing Zhang(张静), Jianxun Su(宿建勋), Yingjie Chen(陈颖杰), Wei Gao(高伟), Zhenwei Wu(吴振伟), EAST Team
Chin. Phys. B, 2019, 28 (**12**): 125202. DOI: 10.1088/1674-1056/ab54b2

Comparative study of boron and neon injections on divertor heat fluxes using SOLPS-ITER simulations

Lei Peng(彭磊)[1], Zhen Sun(孙震)[2], Ji-Zhong Sun(孙继忠)[1,†], Rajesh Maingi[2], Fang Gao(高放)[3], Xavier Bonnin[4], Hua-Yi Chang(常华溢)[1], Wei-Kang Wang(汪炜康)[1], and Jin-Yuan Liu(刘金远)[1]

[1] *Key Laboratory of Materials Modification by Laser, Ion, and Electron Beams (Ministry of Education), Dalian University of Technology, Dalian* 116024, *China*
[2] *Princeton Plasma Physics Laboratory, Princeton, NJ* 08543, *United States of America*
[3] *School of Computer and Communication Engineering, Dalian Jiaotong University, Dalian* 116028, *China*
[4] *ITER Organization, Route de Vinon-sur-Verdon, CS* 90 046, 13067 *St-Paul-lez-Durance, France*

(Received 29 June 2024; revised manuscript received 13 August 2024; accepted manuscript online 20 August 2024)

Based on the EAST equilibrium, the effects of boron (B) and neon (Ne) injected at different locations on the target heat load, and the distributions of B and Ne particles were investigated by transport code SOLPS-ITER. It was found that the B injection was more sensitive to the injection location for heat flux control than impurity Ne. The high electron and ion densities near the inner target in the discharge with impurity B injected from over X-point (R_1) led to plasma detachment only at the inner target, and the localized B ions in the cases with injection from outer target location (R_2) and upstream location (R_3) led to far-SOL detachment at the outer target, but not at the inner target. In contrast, for Ne, the spatial distributions of Ne ions and electrons were found to be similar in all the cases at the three injection locations, and the detached plasma was achieved at the inner target and the electron temperature was reduced at the outer target. For locations R_2 and R_3, impurity B showed a more pronounced effect on the heat flux at the far-SOL of the outer target. Further analysis indicated that Ne atoms came mainly from the recycling sources, whereas B atoms came mainly from injection, and that their distinct atomic distributions resulted from the difference in the ionization threshold and ionization mean free path. In addition, the radiation proportion of B in the divertor region was larger than that of Ne when the total radiation power was similar, which suggests that B has less influence on the core region.

Keywords: boron, neon, injection location, heat flux

PACS: 52.25.Vy, 52.55.Fa, 52.55.Rk, 52.65.–y **DOI:** 10.1088/1674-1056/ad711e

1. Introduction

Active impurity injection is a commonly used method in tokamaks for controlling plasma, improving plasma performance and reducing the divertor heat load.[1–4] The key to active impurity injection is to effectively reduce the edge heat flux while maintaining minimal impact of impurities on the core plasma. Achieving this requires selection of the appropriate working impurity, injection flow rate and injection location.

Nitrogen (N_2), neon (Ne) and argon (Ar) are commonly adopted impurities in tokamak devices to reduce the heat load to the divertor.[5–8] N_2 is not employed in the EAST device mainly due to Li wall conditioning.[9] EAST discharges[10] with applying Ne and Ar injection showed that both Ne and Ar could result in detached plasma as a result of strong impurity radiation. However, Ar injection usually led to more severe impurity accumulation and high radiation power loss compared to the tolerable radiation loss of Ne. Recently, low-Z impurity injection experiments that were carried out in multiple devices[11–17] showed that real-time boron (B) powder injection can improve wall conditions, enhance plasma performance and reduce the divertor heat flux. DIII-D experiments[15] indicated that low-Z impurity injection was a novel and effective method to reduce the divertor heat flux while maintaining good energy confinement. Boron injection experiments in EAST indicated that B can effectively reduce the divertor heat flux and impurity content in the plasma, and suppress edge localized modes.[16] Thus, both impurities B and Ne show promise for future long-pulse discharges.

Neon is a recycling impurity that can exist in the plasma for a long time, thereby limiting the long-pulse, high-parameter operation of tokamak devices.[18] Compared to B, Ne has a larger negative impact on the core plasma and therefore its injection flow rate must be carefully controlled. In contrast, B is a non-recycling impurity, and its deposition on the wall has beneficial effects on wall conditions. Nonetheless, it may result in fuel retention due to the co-deposition of tritiated borane.[11] In addition, for a non-recycler, the specific injection location may influence the impurity distribution, whereas for a recycling impurity, the initial injection location may not matter.[18] The different properties of these two impurities may lead to different effects on the plasma properties. Thus, it is necessary to conduct in-depth research.

Although previous studies have investigated the effects of B and Ne injection separately, a comprehensive comparative

†Corresponding author. E-mail: jsun@dlut.edu.cn

© 2024 Chinese Physical Society and IOP Publishing Ltd

study of their impacts on divertor heat flux and plasma performance is lacking. Such a comparison is crucial for optimizing impurity injection strategies in current and future fusion devices. Moreover, the underlying mechanisms governing the B and Ne behavior, such as their atomic and radiation properties, are not yet fully understood.

This study, based on discharge data from EAST experiments, focuses on investigating the influence of B and Ne impurities on the divertor target heat flux using the transport code SOLPS-ITER.[19–21] By analyzing impurity distribution and radiation, the physics behind the different impacts on the heat flux to the divertor between the two impurities is explored.

2. Simulation details

In this study, the density and temperature profiles were reconstructed from the discharge data of EAST #85043, with upper single null configuration and favorable toroidal magnetic direction ($\boldsymbol{B}\times\nabla\boldsymbol{B}$ towards the upper X-point). The simulated grid, as shown in Fig. 1, includes quadrilateral grids for tracing charged particles and triangular grids for tracing neutral particles. Three impurity injection locations, $R_1 = 1.57$ m, $R_2 = 1.73$ m and $R_3 = 1.95$ m, marked by the red arrows in Fig. 1, were selected for simulations. Location R_1 corresponds to the location for B impurity injection experiments in the EAST device[16,17,22] and is located to the left above the X-point; location R_2 corresponds to the injection position used in Ne impurity injection experiments[23] and is located at the outer scrape-off layer (SOL), approximately 5 cm away from the outer strike point; location R_3 is employed in the experimental injection of lithium powder,[24] specifically through the upper divertor gap, which can be regarded as an upstream position.

The following boundary conditions were set according to the experimental data. At the core boundary, 4.0 cm inside the separatrix at the outer midplane (OMP), the density of deuterium ions was fixed at 4.0×10^{19} m^{-3}. The power entering the computational domain from the core boundary was 3.2 MW, and divided equally into ion and electron channels. Pumps considered in the simulation include the cryopump and the pumping port-end. The former had a recycling coefficient of 0.94, indicated by the blue line in Fig. 1; the latter had a recycling coefficient of 0.99 and is denoted by the orange line.[25] To simulate the edge transport barrier of the H-mode discharge, the radial transport coefficients were reduced in this region. The radial particle and thermal diffusivity coefficients are shown in Fig. 2, and the thermal diffusivity coefficients are the same for ions and electrons. Table 1 summarizes the recycling coefficient for the cases without impurity, and with B and Ne, except for the pumps. The neutrals in the case without impurity injection include D atoms and D_2 molecules, and include impurity atoms in the cases with impurity injection. In the case without impurity injection, the recycling coefficient for neutrals and ions was 1, meaning that all particles hitting the wall return to the plasma in neutrals. The same value applies to the cases with Ne injection. For impurity B, experimental results indicate that it has some effect on recycling.[17] As a result, the recycling coefficient for D ions was taken to be 0.98 at the inner and outer targets, and for B ions was assumed to be 0.3. In fact, the two impurities, B and Ne, are injected, respectively, by impurity powder dropper and gas puffing. However, this work focuses on comparing the effects of the two impurities themselves on the background plasma properties and, therefore, ignores the different injection methods of the two impurities.

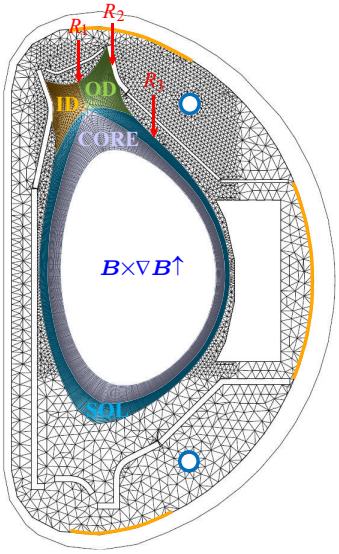


Fig. 1. The mesh used in simulation. Three injection locations are marked by red arrows. The quadrilateral meshes include inner (ID) and outer (OD) divertors, a core region (CORE) and a scrape-off layer (SOL). The two cryopumps are marked by blue circles and the pumping port-ends are shown in orange lines.

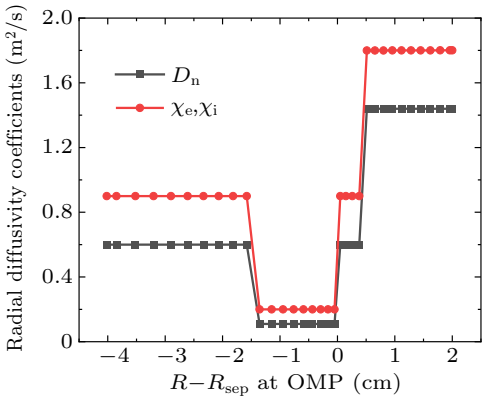


Fig. 2. Radial particle (D_n) and thermal (χ_e and χ_i) diffusivity coefficients at the outer midplane.

Table 1. The recycling coefficients in the cases with no impurity injection, and with B and Ne injection, except on the pumps. The value, 0.98, in parenthesis represents the recycling coefficient of D ions at the targets.

	Neutrals	D ions	B ions	Ne ions
No impurity	1.0	1.0	–	–
B injection	1.0	1.0 (0.98)	0.3	
Ne injection	1.0	1.0	–	1.0

The injection flow rate of Ne was set at 1.0×10^{20} atoms/s based on experimental parameters[23] for all three injection locations. To compare the effects of B with those of Ne, the total radiation in each case with B impurity injection was similar to the corresponding case with Ne injection (as shown in Table 2). Total radiation includes the line, bremsstrahlung, and neutral radiation from the main and impurity particles. In this way, the B powder flow rates were determined to be 7.0×10^{20}, 2.6×10^{21} and 2.7×10^{21} atoms/s, respectively, at locations R_1, R_2 and R_3. Unless otherwise specified, all the simulation results in the present study are based on these flow rates. In addition, to reproduce a realistic discharge, the $\boldsymbol{E}\times\boldsymbol{B}$ drift was included in all the simulations. Considering that there is only a mild effect of diamagnetic drift[25] on the temperature and heat flux at the target, the diamagnetic drift was not included in the present study.

3. Simulation results

3.1. Heat fluxes to targets

The heat flux to the divertor can be reduced via impurity radiation by injecting either B or Ne. Consequently, plasma-wall interaction can be mitigated and the sputtering of wall materials can therefore be alleviated. Figures 3 and 4 present the temperature and heat flux profiles at the inner and outer targets, respectively. In the case of pure D discharge, the temperature and heat flux at the inner target are lower than those at the outer target, which is consistent with experimental and other simulation results.[26–28]

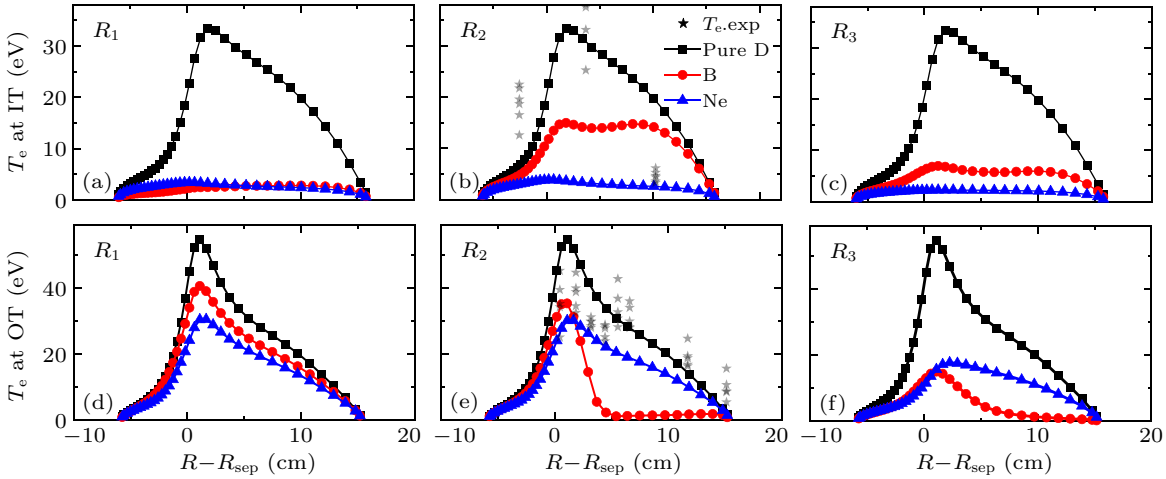


Fig. 3. Temperature profiles at the inner (IT) and outer (OT) targets for three injection locations. The three injection locations (R_1, R_2 and R_3) refer to Fig. 1. Black lines are for no impurity injection; red lines are for B injection; blue lines are for Ne injection. The injection rate of Ne is set at 1.0×10^{20} atoms/s for all the locations, and the B flow rates at locations R_1, R_2 and R_3 are 7.0×10^{20}, 2.6×10^{21} and 2.7×10^{21} atoms/s, respectively. Star symbols in the middle panels are the experimental target T_e measured by Langmuir probes in pure D discharge. These injection parameters are the same for all the following figures.

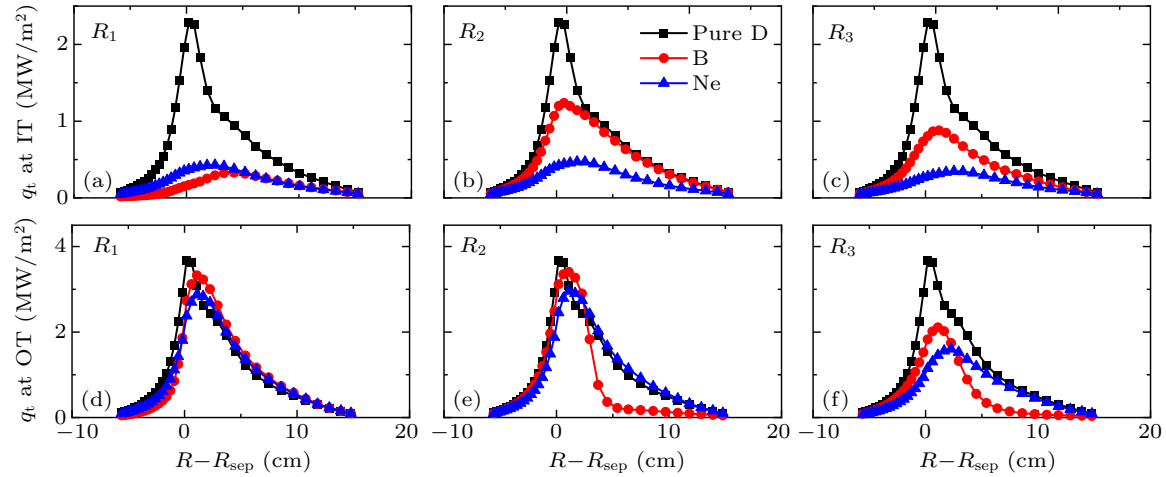


Fig. 4. Heat flux profiles at the inner (IT) and outer (OT) targets for pure D discharge, B and Ne impurity injection discharges at the three injection locations.

As shown in Figs. 3 and 4, at injection location R_1, both B and Ne reduce the heat flux significantly at the inner target with similar profiles. At the same time, both peak temperatures fall below 5 eV, indicating that plasma detachment has been achieved at the inner target. At the outer target, with B (Ne) injection, the temperatures drop from 55 eV to 41 eV

(31 eV) and the heat fluxes decrease by 9.8% (22%). At injection location R_2, the temperature at the inner target drops from 55 eV to around 4 eV with Ne injection, and plasma detachment is achieved. The decrease in temperature or heat flux at the inner target in the case of Ne injection is much larger than in the B injection. For the outer target, the temperature and heat flux peaks with B and Ne injections are close. However, a significant difference between B and Ne injection is the temperature and heat flux in the far-SOL region at the outer target. In the case with B injection, the temperature and heat flux in the outer far-SOL region reduce significantly, and far-SOL detachment is achieved at the outer target. In contrast, far-SOL detachment is not observed anywhere near the outer target in the case with Ne injection. At location R_3, the effects of B and Ne injection on the temperature and heat flux profiles are similar to those injected at location R_2, but the reduction in both heat flux and temperature are more pronounced at this injection location.

From Figs. 3 and 4, no significant difference in both temperature and heat flux profiles at the inner and outer targets is observed for Ne injection cases, except that injection at R_3 leads to the lowest temperature and heat flux peaks at the outer target. For the B injection cases, the peaks and profile shapes of the temperature and heat flux at the outer and inner targets are significantly different. Plasma detachment at the inner target is only achieved at location R_1, and a noticeable local effect on the profiles at the outer target is observed for the cases at locations R_2 and R_3. Therefore, the influence of impurity B on the background plasma is more susceptible to the injection location, whereas the injection location has little effect on impurity Ne. In a previous Ne seeding study,[29] it was found that the seeding location has a minimal effect on divertor performance.

3.2. Radiation

The reduction in either temperature or heat flux is achieved through impurity radiation. To explore the reasons for the different temperature and heat flux profiles in the cases with B and Ne injected at different locations, the distribution of impurity radiation is therefore analyzed. Figure 5 shows the two-dimensional distribution of radiation power density by impurities B and Ne. It is observed from the figure that with injection location R_1, the B radiation is concentrated mainly in the inner divertor, which explains the significant reduction in both heat flux and temperature at the inner target (Figs. 3 and 4). In contrast, radiation in the outer divertor is relatively weak and is concentrated mostly in the private flux region (PFR). Correspondingly, small changes are observed in the temperature and heat flux profiles at the outer target shown in Figs. 3 and 4. At injection location R_2, the B radiation is distributed mainly near the injection location in the outer divertor, leading to a significant decrease in temperature in the far-SOL region, and far-SOL detachment (as shown in Fig. 3). Although the radiation also increases near the outer strike point, it is not enough to achieve detachment there and the electron temperature is reduced to ~ 35 eV compared to the pure D case. At location R_3, the B radiation region extends from the injection location along the neighboring magnetic flux tube towards the outer target, leading to a significant decrease in temperature in the far-SOL region. Compared to location R_2, the lower temperature at the outer target for B injection at location R_3 is attributed to the enhanced radiation in the SOL.

Comparatively, the distributions of Ne radiation are similar at the three injection locations. However, at location R_3, the radiation near the separatrix in the divertor region, especially in the inner divertor, is significantly higher than at other locations. In addition, the Ne radiation in the core region is significantly higher than the B radiation, indicating that the effect of Ne on the core region is greater than that of impurity B. Further analysis of the radiation distribution validates that the contributions of impurity B are influenced more strongly by the injection location.

Table 2 summarizes the radiation powers in specific regions for the three injection locations R_1, R_2 and R_3. The regions, as shown in Fig. 1, include the core region, SOL, outer divertor (OD), inner divertor (ID) and the whole domain (total). Radiation powers consist of the line, bremsstrahlung and neutral radiation. The radiation in the divertor region in the cases with Ne injected at locations R_1, R_2 and R_3 accounts for 61.5%, 62.3% and 54.4% of the whole domain, respectively, while the corresponding percentages for the cases with B injection are 94.8%, 95.1% and 32.2%, respectively. The proportions of radiation in the divertor regions with injection locations R_1 and R_2 are similar, while the proportions of divertor radiation decrease at location R_3, especially for the case with B injection. From this table, we learn that impurity injected in the divertor region either at R_1 or R_2 is more beneficial for increasing the divertor radiation in the divertor region, whereas injection in upstream plasma, e.g., location R_3, leads to more radiation in the core region and SOL.

Comparing the two impurities injected at locations R_1 and R_2, radiation in the cases with B injection is well concentrated in the divertor region, whereas the Ne injection cases have a larger proportion of radiation in the core and SOL regions. This means that impurity Ne reduces the heat flux flowing into the divertor region by dissipating energy upstream. At location R_3, the proportion of radiation in the divertor region for the B injection case decreases significantly, compared with at locations R_1 and R_2, while for the Ne case, it decreases only

slightly. This also indicates that the injection location has a significant impact on B distribution. For impurity Ne, large radiation power is always present in the inner divertor regardless of the injection location, and this is responsible for the detached plasma near the inner target. Furthermore, the radiation of the B injection cases in the core region is at least 2.4 times smaller than that of the Ne cases when the radiation powers of B and Ne cases are similar.

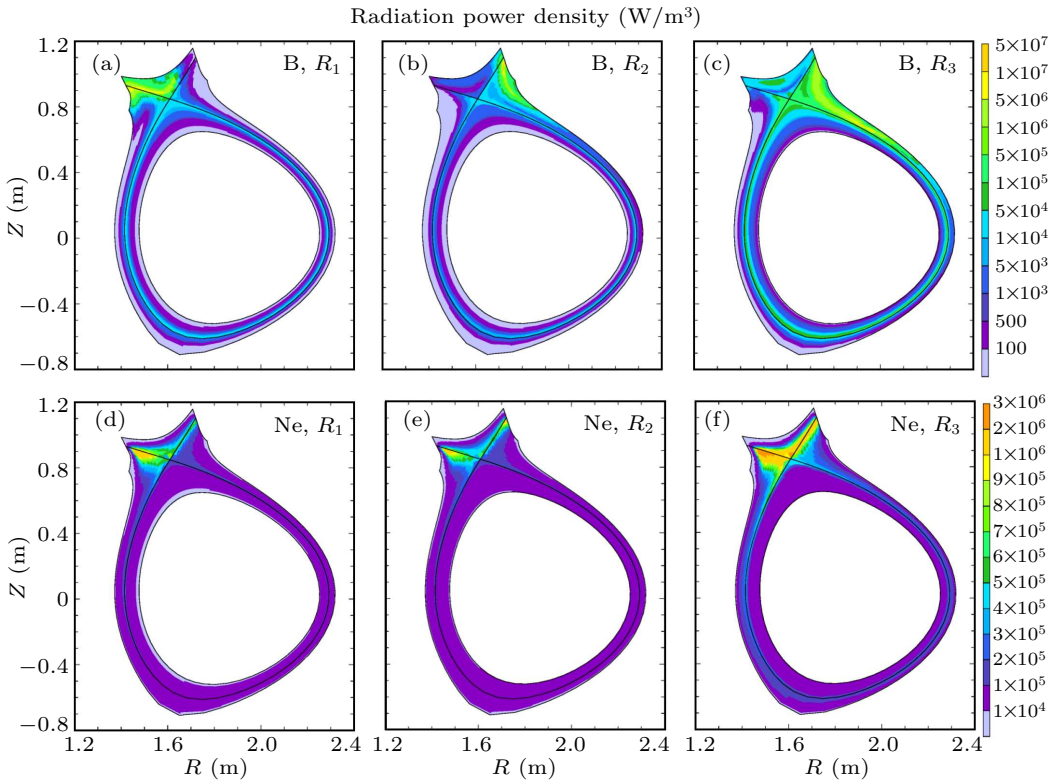


Fig. 5. Radiation power density by B and Ne at injection locations R_1, R_2 and R_3. The top row is for B, and the bottom row is for Ne. The flow rates of Ne are all 1.0×10^{20} atoms/s, and the flow rates of B at locations R_1, R_2 and R_3 are 7.0×10^{20}, 2.6×10^{21} and 2.7×10^{21} atoms/s, respectively.

Table 2. Radiation powers in the core region, SOL, outer divertor (OD), inner divertor (ID) and the whole domain. The unit of radiation power is kW.

	Impurity	Core	SOL	OD	ID	Total
$R=1.57$	Ne	84	139	124	232	579
	B	17	14	125	438	594
$R=1.73$	Ne	76	122	133	194	525
	B	13	13	452	57	535
$R=1.95$	Ne	172	306	259	312	1049
	B	71	643	252	87	1053

The impurity radiation power in plasma can be evaluated by the formula $P_{\rm rad} = n_{\rm e}\sum_Z n_Z \sum_Z (\zeta_Z L_Z(T_{\rm e}))$, in which $n_{\rm e}$ and n_Z represent the electron and impurity densities, respectively, ζ_Z represents the relative density of different impurity charge states, and $L_Z(T_{\rm e})$ is the cooling factor, describing the temperature-dependent radiation capacity of impurity.[30] First, the distribution of electron density in cases with either impurity B or Ne impurity injection is shown in Fig. 6. For Ne injection, the distributions of electron density at different locations are similar, with a significantly higher electron density observed near the inner target in the near-SOL region. Therefore, at different injection locations, neon radiation is determined mainly by its extensive distribution of Ne ions. For B impurity, the electron density near the target, especially the inner target, is significantly higher in all three cases. In addition, the broadened high-density region (1.0×10^{20}–2.0×10^{20} m^{-3}) next to the inner target in the case at injection location R_1 is more noticeable than the other two cases. In both the Ne and B injection cases, the high electron density near the inner target is associated with the $\boldsymbol{E}\times\boldsymbol{B}$ drift. For the case with B injected at location R_1, the injection location is beneficial for enhancing the electron density near the inner target, compared with injection locations R_2 and R_3.

Figure 7 shows the cooling factors of species B and Ne in the coronal equilibrium, taken from the ADAS database.[31] It is found that the cooling factor of species B is significantly higher than that of Ne when the temperature is below 10 eV, while the cooling factor of species Ne is higher in the range of $\sim$ 10–100 eV, with a peak at $\sim$ 30 eV. This indicates that impurity B is conducive to cooling the plasma in the low-temperature regions, while impurity Ne plays a larger role in cooling the plasma in high-temperature regions, which is the reason for the larger fraction of B radiation in the divertor region (as shown in Table 2). In what follows, we will discuss the features of their distributions.

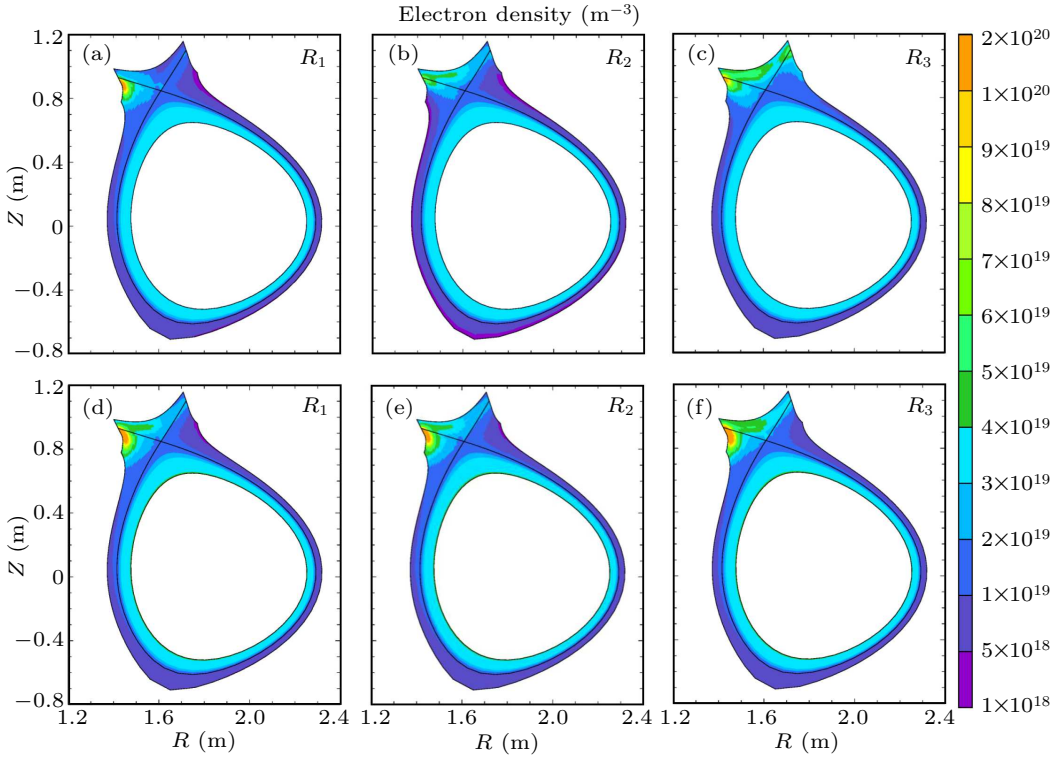


Fig. 6. Electron density in the cases with B and Ne injected at R_1, R_2 and R_3 locations. The top row is for B and the bottom row is for Ne. The flow rates of Ne are all 1.0×10^{20} atoms/s and the flow rates of B at locations R_1, R_2 and R_3 are 7.0×10^{20}, 2.6×10^{21} and 2.7×10^{21} atoms/s, respectively.

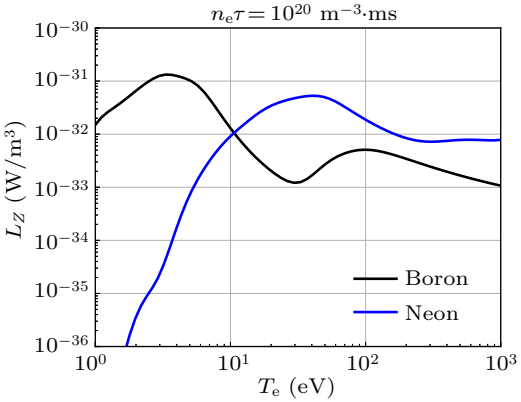


Fig. 7. The cooling factors of impurities B and Ne versus electron temperature.

3.3. Impurity distribution

The two-dimensional distributions of all B and Ne ions are shown in Fig. 8. In the case of injection location R_1, B ions are distributed mainly near the separatrix in the inner divertor. In the case of injection location R_2, they are distributed primarily near the injection location, with localized diffusion along the poloidal and radial directions. In the case of injection location R_3, they move along magnetic field lines towards the outer target and diffuse in the radial direction from the injection location; some of the B ions are transported to the inner divertor, driven mainly by $\boldsymbol{E}\times\boldsymbol{B}$ drift. The distribution of B ions is strongly related to the injection location. For Ne, its ions are distributed mainly in the divertor region, and the Ne density in the inner divertor is slightly higher than that in the outer divertor due to $\boldsymbol{E}\times\boldsymbol{B}$ drift. Although the distribution of Ne ions is also influenced by the injection location, the influence is not as significant as that on B ions. In addition, the density of Ne ions in the divertor region and upstream at location R_3 is significantly higher than that at the other two injection locations.

After comprehensively considering the electron density, cooling factor and impurity ions, we can explain the distribution of radiation. For B impurities, at location R_1, both the high electron density and impurity ion density near the inner target result in enhanced radiation. The low temperature at the inner target (see Fig. 3) implies that the temperature drops easily to the low-temperature region, leading to an increase in the cooling factor and further enhancement of radiation until plasma detachment is achieved. At locations R_2 and R_3, impurity ions are concentrated in the outer divertor and the vicinity of the injection location, with only a small number of impurities entering the inner divertor region. As a result, the small impurity radiation in the inner divertor is not sufficient to facilitate plasma detachment. At the outer target, the high impurity density in the far-SOL region leads to high radiation in a localized zone, as shown in Fig. 5. In addition, the electron temperature at the outer target is higher than the inner target, especially at the outer strike point, and thus only far-SOL detachment is achieved. For impurity Ne, regardless of the injection location, both the electron density and impurity density near the inner target plate are relatively high, facilitating plasma detachment.

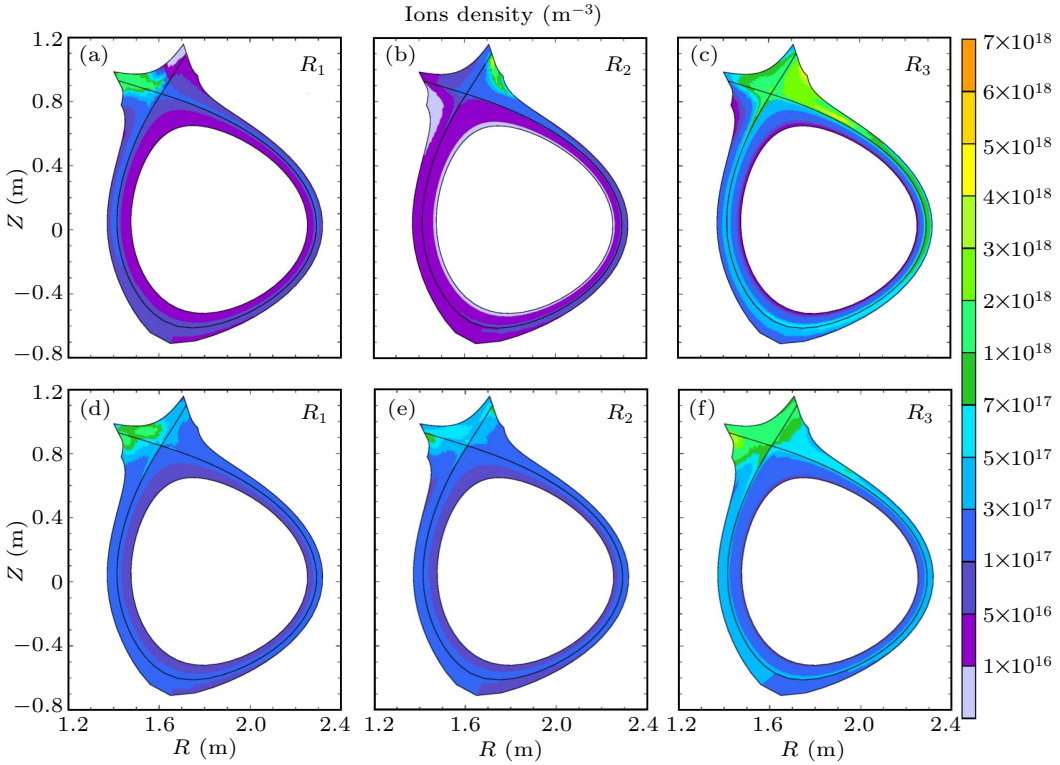


Fig. 8. Densities of all B and Ne ions at R_1, R_2 and R_3 injection locations. Top row is for B and the bottom row is for Ne. The flow rates of Ne are all 1.0×10^{20} atoms/s and the flow rates of B at locations R_1, R_2 and R_3 are 7.0×10^{20}, 2.6×10^{21} and 2.7×10^{21} atoms/s, respectively.

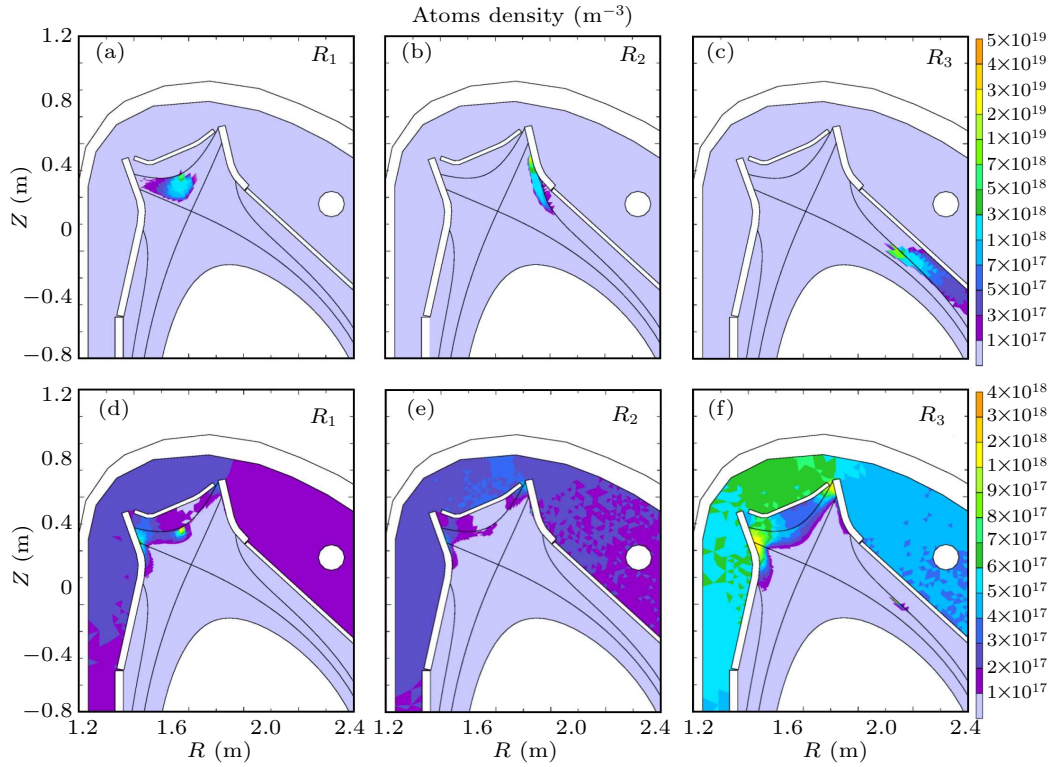


Fig. 9. Density of B and Ne atoms at R_1, R_2 and R_3 injection locations. Top row is for impurity B and the bottom row is for impurity Ne. The flow rates of Ne are always 1.0×10^{20} atoms/s and the flow rates of B are 7.0×10^{20}, 2.6×10^{21} and 2.7×10^{21} atoms/s, respectively, for the cases at locations R_1, R_2 and R_3.

The distribution of impurity ions is closely related to the distribution of atoms, which is shown in Fig. 9. B atoms are distributed mainly near the injection location, while most Ne atoms are concentrated in the divertor region, and numerous Ne atoms escape from the plasma. When Ne is injected from location R_3, the atomic density is significantly larger than at locations R_1 and R_2. The distribution of B atoms is more concentrated at the injection location, while in contrast, Ne atoms

are present mainly in the divertor region, which is less affected by the injection location. The distributions of ions in Fig. 8 can be easily understood from the atomic distributions, and the reason for such a significant difference in the distribution of B and Ne atoms will be explored further in the discussion section.

Table 3. Atomic sources from injection (impurity flow rate) and recycling at the plasma facing wall (including the inner (IT) and outer (OT) targets, the first wall (FW), the dome wall (DW) and the whole wall surface (total)). The unit of atomic sources is 1.0×10^{19} atoms/s.

	IT	OT	FW	DW	Total	Injection
R_1-B	54.2	2.7	5.5	2.5	64.9	70
R_2-B	1.1	148.7	8.1	1.7	159.6	260
R_3-B	16.0	165.0	39.1	14.8	234.9	270
R_1-Ne	47.8	30.4	4.8	2.1	85.1	10
R_2-Ne	31.0	53.1	4.0	1.9	90.0	10
R_3-Ne	101.3	88.3	12.5	3.9	206.0	10

Table 3 summarizes the atomic sources at plasma-facing walls from recycling and the injected atomic source to understand the reasons for the difference in the distribution of B and Ne atoms. The recycled atomic sources are calculated from all impurity ions and atoms hitting the wall. From this table, it can be observed that for Ne atomic sources, the injected atomic source is at least eight times smaller than the recycling atomic source. Therefore, Ne atoms in the plasma come mainly from the recycled atomic sources in the divertor. This is the reason the distribution of Ne is not significantly affected by the injection location. The previous Ne seeding experiments conducted on EAST[32] indicated that Ne radiation was induced dominantly by recycling impurities from the divertor targets, rather than the injected impurities, which is consistent with our simulation results. In addition, impurity Ne injected from location R_3 is more likely to enter the core region, and the high temperature facilitates impurity ionization, leading to higher Ne ion density upstream. The high Ne ion flux transported to the wall produces a larger density of recycled Ne atoms (as shown in Fig. 9(f)), which results in a higher Ne ion density in the divertor region (as shown in Fig. 8(f)). For B atoms, the source from injection exceeds that from recycling, and the recycled source is influenced significantly by the injection location. Therefore, the distribution of B atoms is determined mainly by the injection location. Hence, there is a considerable difference in the reduction of heat flux at different injection locations for impurity B. This also explains the difference between the sensitivities of B and Ne to the injection location.

4. Discussion

From the simulation results, we know that the electron temperature at the targets and the heat flux to the divertor targets are strongly influenced by the distribution of impurities. As is well known, the ion distribution is closely correlated with the atomic distribution, and the distribution of the latter is strongly related to its ionization threshold and plasma conditions.

The neutral impurity particles come mainly from the recycling and the injected impurity. Impurity atoms and ions that hit the wall return to the plasma in the form of neutral atoms, known as recycled atoms. These recycled atoms move back and forth between the plasma and the wall until they are ionized. The trajectory of a neutral atom strongly depends on a characteristic parameter, the ionization mean free path:[33,34]

$$\lambda_{\mathrm{ion},a}^{\mathrm{mfp}} = v_a/(n_\mathrm{e}\langle\sigma v\rangle_{\mathrm{ion},a}), \tag{1}$$

in which v_a represents the average velocity of atom a, which we can roughly take as a constant, n_e is the electron density and $\langle\sigma v\rangle_{\mathrm{ion},a}$ denotes the ionization rate coefficient of atom a. The ionization rate coefficient strongly depends on the localized plasma temperature. As a result, the ionization mean free path is significantly influenced by the temperature and density of electrons. The ionization rate coefficients of atoms B and Ne versus temperature at electron density of 1.0×10^{19} m^{-3} are shown in Fig. 10. The ionization rate coefficient of Ne is always less than that of B, especially in the low-temperature range, e.g., under 10 eV, where the Ne ionization rate coefficient is at least 1 order of magnitude smaller than that of B atoms.

Taking the case with injection location R_1 as an example, the ionization mean free path is further analyzed for impurities Ne and B. The velocities of neutral atoms are similar in the divertor region and the electron density is also similar, as shown in Fig. 6. Thus, the difference between their ionization mean free paths can be estimated by their ionization rate coefficients, as shown in Fig. 10. From Eq. (1), we know that the ionization mean free path of Ne is much larger than that of B in the low-temperature range. For instance, at the inner and outer strike points, λ^{mfp} of Ne is ~ 40 and ~ 6 times larger than that of B atoms. This implies that Ne atoms diffuse over a much wider region than B atoms.

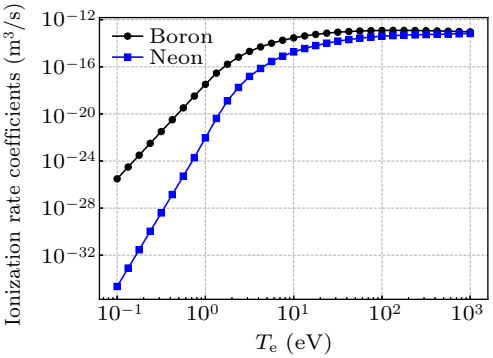


Fig. 10. Ionization rate coefficients of atoms B (from "year 89" ADAS database) and Ne, with electron density of 1.0×10^{19} m^{-3}.

Now, we attempt to understand the distribution of impurity atoms. Neon atoms are ionized after injection from loca-

tion R_1, and the ions are transported along the magnetic field lines to the divertor targets (especially the inner target), and simultaneously the radiation induced by the impurity results in a decrease in temperature. The long ionization mean free path of the recycled Ne atoms leads to the extensive presence of Ne atoms. In the private flux region and in the vicinity of the inner target, the electron temperature is low (as shown in Fig. 11), mostly below 20 eV, and Ne atoms (mainly from recycled sources), whose ionization threshold is as high as 21.6 eV, are therefore present extensively in the private flux region and near the inner target, as shown in Fig. 9. In addition, from the same figure, we can see that numerous Ne atoms enter the vacuum chamber due to the long ionization mean free path of Ne atoms and the pumping effect of the pumps.

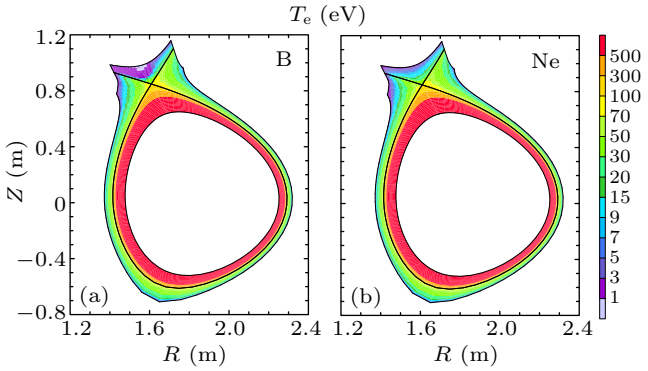


Fig. 11. Electron temperature in the cases with impurities B (a) and Ne (b) injection at location R_1.

For B atoms, the ionization mean free path is relatively short. After the ionization of B atoms near the injection location, the B ions exist locally. Recycled B atoms from the ions transported along the magnetic field lines to the targets are also distributed locally. The recycled B atoms ionize easily due to the low ionization threshold of 8.3 eV, resulting in a low atomic density near the targets. Consequently, most B atoms are concentrated near the injection location, and are significantly influenced by the injection location. This suggests that selecting an appropriate injection location for B is critical for modulating the localized plasma effectively.

5. Conclusion

Based on the equilibrium of EAST discharge #85043, the impact of B and Ne impurities on the divertor heat flux in the favorable toroidal magnetic field direction was studied using the edge plasma code SOLPS-ITER. The simulation results indicate that when impurity B is injected from the X-point location (R_1), it is easy to achieve detachment for the inner target at a low flow rate, and that from the outer target (R_2) and upstream (R_3) locations leads to far-SOL detachment at the outer target. For Ne impurity, injection from different locations consistently results in plasma detachment at the inner target.

The analysis of radiation revealed that B radiation is influenced significantly by the injection location, whereas Ne radiation distribution depends weakly on the injection location. When impurity B was injected at location R_1, plasma detachment was achieved at the inner target, primarily due to the high electron density and impurity density near the inner target, as well as the low background temperature. At locations R_2 and R_3, the far-SOL detachment at the outer target is mainly related to the localized B ions. For Ne impurity, a similar distribution of impurity radiation is observed at different injection locations due to the electron and impurity densities being less affected by the injection location. The larger cooling factor of B impurity in low-temperature results in the greater proportion of radiation from impurity B in the divertor region than that from impurity Ne. This suggests that impurity B may reduce the heat flux effectively while having a smaller impact on the core plasma.

The distribution of impurity ions is closely related to their atoms. Analysis of the atomic sources indicates that the B atoms come mainly from the injection source, while the Ne atoms come mainly from recycling. The reduction in heat flux by impurity B is therefore more easily influenced by the injection location, whereas that by impurity Ne is less sensitive to the injection location. The extensive distribution of Ne atoms in the divertor region is related to their recycling property, high ionization threshold and long ionization mean free path, while the localized distribution of B ions near the injection location is due to their low ionization threshold and short ionization mean free path.

Acknowledgements

Project supported by the National Key R&D Program of China (Grant No. 2019YFE03030004), the National Natural Science Foundation of China (Grant No. 12275040), and the Users with Excellence Program of Hefei Science Center CAS (Grant No. 2020HSC-UE010). This research is also sponsored in part by the U.S. Department of Energy under contract DE-AC02-09CH11466. The authors thank the Supercomputing Center of Dalian University of Technology for providing some computational resources. The views and opinions expressed herein do not necessarily reflect those of the ITER Organization.

References

[1] Xiao W W, Diamond P H, Zou X L, *et al*. 2012 *Nuclear Fusion* **52** 114027
[2] Lunsford R, Hu J S, Sun Z, *et al*. 2018 *Nuclear Fusion* **58** 126021
[3] Lang P T, Maingi R, Mansfield D K, *et al*. 2017 *Nuclear Fusion* **57** 016030
[4] Reimold F, Wischmeier M, Bernert M, *et al*. 2015 *Nuclear Fusion* **55** 033004
[5] Kallenbach A, Dux R, Fuchs J C, *et al*. 2010 *Plasma Physics and Controlled Fusion* **52** 055002

[6] Nakano T 2015 *Journal of Nuclear Materials* **463** 555
[7] Bernert M, Wischmeier M, Huber A, *et al*. 2017 *Nuclear Materials and Energy* **12** 111
[8] Pitts R A, Bonnin X, Escourbiac F, *et al*. 2019 *Nuclear Materials and Energy* **20** 100696
[9] Li L, Zhang D H, Meng X C, *et al*. 2021 *Nuclear Materials and Energy* **28** 101049
[10] Li K, Lin X, Yang Z, *et al*. 2023 *Nuclear Fusion* **63** 026025
[11] Lunsford R, Rohde V, Bortolon A, *et al*. 2019 *Nuclear Fusion* **59** 126034
[12] Kawate T, Ashikawa N, Goto M, *et al*. 2022 *Nuclear Fusion* **62** 126052
[13] Gilson E P, Lee H H, Bortolon A, *et al*. 2021 *Nuclear Materials and Energy* **28** 101043
[14] Bodner G, Gallo A, Diallo A, *et al*. 2022 *Nuclear Fusion* **62** 086020
[15] Effenberg F, Bortolon A, Casali L, *et al*. 2022 *Nuclear Fusion* **62** 106015
[16] Sun Z, Diallo A, Maingi R, *et al*. 2021 *Nuclear Fusion* **61** 014002
[17] Maingi R, Hu J S, Sun Z, *et al*. 2020 *Journal of Fusion Energy* **39** 429
[18] Stangeby P C 2000 *The Plasma Boundary of Magnetic Fusion Devices* (Boca Raton)
[19] Schneider R, Bonnin X, Borrass K, *et al*. 2006 *Contributions to Plasma Physics* **46** 3
[20] Chankin A V, Coster D P, Dux R, *et al*. 2006 *Plasma Physics and Controlled Fusion* **48** 839
[21] Bonnin X, Dekeyser W, Pitts R, *et al*. 2016 *Plasma and Fusion Research* **11** 1403102
[22] Xu W, Hu J S, Sun Z, *et al*. 2021 *Physica Scripta* **96** 124034
[23] Wang R, Yang Z, Li K, *et al*. 2022 *Physics of Plasmas* **29** 112502
[24] Sun Z, Maingi R, Hu J S, *et al*. 2019 *Nuclear Materials and Energy* **19** 124
[25] Jia G, Wang H, Xu G, *et al*. 2022 *Nuclear Fusion* **62** 056005
[26] Ma X, Wang H Q, Guo H Y, *et al*. 2021 *Nuclear Fusion* **61** 054002
[27] Xu J C, Wang L, Wang H Q, *et al*. 2021 *Nuclear Fusion* **61** 096004
[28] Paradela Pérez I, Groth M, Wischmeier M, *et al*. 2019 *Nuclear Materials and Energy* **19** 531
[29] Park J S, Bonnin X, Pitts R, *et al*. 2024 *Nuclear Fusion* **64** 036002
[30] Tokar M Z 2008 *Fusion Science and Technology* **53** 243
[31] OPEN-ADAS, https://open.adas.ac.uk/
[32] Xu G S, Yuan Q P, Li K D, *et al*. 2020 *Nuclear Fusion* **60** 086001
[33] Groth M, Andrew P, Fundamenski W, *et al*. 2002 *Nuclear Fusion* **42** 591
[34] Chrobak C P, Stangeby P C, Hollmann E, *et al*. 2018 *Nuclear Fusion* **58** 106019